On the Propagation of Free Topographic Rossby Waves near Continental Margins. Part 1: Analytical Model for a Wedge[1]

HSIEN WANG OU[2]

WHOI/MIT Joint Program in Oceanography, Woods Hole, MA 02543

(Manuscript received 10 December 1979, in final form 21 March 1980)

ABSTRACT

An analytical model has been constructed to study the propagation of free waves of subinertial frequency in an infinite wedge filled with a uniformly stratified fluid. The problem is found to transform into the corresponding surface gravity wave problem in a nonrotating homogeneous fluid with the roles of the surface and bottom boundaries interchanged. Analytical solutions are thus available for waves that are either progressive or trapped in the cross-wedge direction, forming respectively continuous and discrete spectra in frequency space. The separation occurs when the nondimensional wave frequency σ (scaled by the inertial frequency f) equals the Burger number S, defined here as $(N/f)\tan\theta^*$, where N is the Brunt-Väisälä frequency and $\tan\theta^*$ is the bottom slope. Since an infinite wedge has no intrinsic length scale, the only relevant nondimensional parameters are the wave frequency σ and the Burger number S. Thus, stratification and bottom slope play the same dynamical role, and the analysis is greatly simplified.

For the progressive waves, asymptotic solutions are obtained for both the far field and small S. Since the surface boundary condition is neglected in the far field, the solution there is similar to the edge wave solution found by Rhines (1970) in an infinitely deep ocean. The asymptotic solution for small S, on the other hand, clearly shows the refraction phenomenon and the presence of amplitude minimum as the apex is approached. Since the asymptotic solutions check very well with the calculations of the general solution, the qualitative behavior of the progressive waves are fairly predictable over the parameter range $S \leqslant O(1)$. The various wave properties associated with the general solution can be understood to a great extent by assuming quasi-geostrophy. The rigid upper surface is found to account for the onshore heat flux generated by these incoming waves.

For the trapped waves, the eigenfrequencies decrease when S decreases and approach the value $(2n + 1)^{-1}$ when S approaches zero where n is the mode number. The modal structure broadens as S increases to some critical value above which no such coastally trapped modes exist.

1. Introduction

There have been considerable efforts (e.g., Thompson, 1971; Rhines, 1971; Thompson and Luyten, 1976) directed toward finding the evidence for bottom intensified topographic Rossby waves since they were first proposed in theory by Rhines (1970). Recently, after an extensive analysis of the current meter data obtained near site D (39°10'N, 70°W), Thompson (1977) concluded that the low-frequency motions there are dominated by linear topographic Rossby wave dynamics. Furthermore, the observed offshore phase propagation is consistent with the assumption that these waves are generated offshore and radiate their energy shoreward toward the shelf. Since the analytic solutions of Rhines (1970) are valid only when the bottom slope is small or the ocean is infinitely deep, they do not apply to the slope region where the bottom slope is typically one or two orders of magnitude greater than that over the continental rise.

To extend Rhines' analysis to a finite-slope and finite-depth regime, we consider in this paper (Part 1) the propagation of free topographic Rossby waves in a wedge filled with a uniformly stratified fluid. The problem is found to be mathematically identical to the corresponding surface gravity wave problem in a nonrotating homogeneous fluid with the roles of the surface and bottom boundaries interchanged. Analytical solutions are therefore available for both progressive (Peters, 1952) and trapped waves (Ursell, 1952) and their properties can be studied. Since the progressive waves can channel the kinetic energy of the deep ocean onto the coastal regions, they are important in understanding the process of dynamical coupling across the continental margins. This process, however, will be discussed in more detail in a companion paper (Ou and Beardsley, 1980, Part 2) where a numerical model incorporating realistic topography and bottom friction will be presented. The trapped wave solutions, on the other hand, are

[1] WHOI Contribution No. 4486.

[2] Present affiliation: Department of Physical Oceanography, Woods Hole Oceanographic Institution, Woods Hole, MA 02543.

0022-3670/80/071051-10$06.50

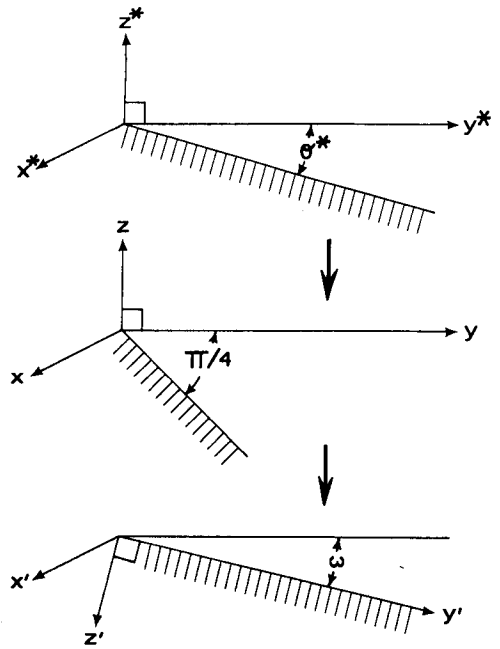

FIG. 1. The wedge in the dimensional, nondimensional and transformed spaces.

important for the understanding of the local oceanic response to the atmospheric forcing near the coast. Coastally trapped waves of subinertial frequency have been found numerically by Wang and Mooers (1976) and Huthnance (1978) for a continuously stratified ocean with a variable bottom. Huthnance has also obtained an analytical solution for the special case of a parabolic bottom and uniform stratification. Our solution is for a different geometry, and some of the general features he has discussed are also observed in our case.

2. The formulation of the model

We consider an infinite wedge filled with a uniformly stratified fluid as shown in the top panel of Fig. 1. The superscript asterisk represents variables in the dimensional space and θ^* is the angle of the wedge. The linearized equations for an inviscid, hydrostatic and Boussinesque fluid are

$$\left.\begin{aligned} u^*_{t*} - fv^* &= -p^*_{x*} \\ v^*_{t*} + fu^* &= -p^*_{y*} \\ 0 &= -p^*_{z*} - \rho^* g \\ u^*_{x*} + v^*_{y*} + w^*_{z*} &= 0 \\ \rho^*_{t*} - \frac{N^2}{g} w^* &= 0 \end{aligned}\right\}, \tag{2.1}$$

where N and f are the Brunt-Väisälä and inertial frequencies, both of which are assumed constant, and g is the gravitational acceleration. Assuming a rigid surface and an impenetrable bottom, the boundary conditions are given by

$$\left.\begin{aligned} w^* &= 0 \quad \text{at} \quad z^* = 0 \\ w^* &= -v^* \tan\theta^* \quad \text{at} \quad z^* = -y^* \tan\theta^* \end{aligned}\right\}. \tag{2.2}$$

Nondimensionalized by the scalings

$$\left.\begin{aligned} (x^*,y^*,z^*) &= L(x,y,z\tan\theta^*) \\ (u^*,v^*,w^*) &= V(u,v,w\tan\theta^*) \\ t^* &= f^{-1}t \\ p^* &= (fVL)p \\ \rho^* &= \left(\frac{fV}{g\tan\theta^*}\right)\rho \end{aligned}\right\}, \tag{2.3}$$

and assuming a solution of the form

$$p \sim p(y,z)e^{i(kx-\sigma t)}, \tag{2.4}$$

the problem is reduced to solving the equations

$$p_{yy} - k^2 p + \frac{1-\sigma^2}{S^2} p_{zz} = 0, \tag{2.5}$$

$$p_z = 0 \quad \text{at} \quad z = 0, \tag{2.6}$$

$$p_z = -\frac{S^2}{1-\sigma^2}\left(p_y + \frac{k}{\sigma}p\right) \quad \text{at} \quad z = -y. \tag{2.7}$$

In the above equations, V is the velocity scale, L can be any length scale, and $S = (N/f)\tan\theta^*$ is the Burger number. Since an infinite wedge has no intrinsic length scale, the only relevant parameters are the nondimensional wave frequency σ and the Burger number S. Hence, stratification and bottom slope play the same dynamical role and the analysis is greatly simplified.

For $0 < \sigma < 1$, we can map this wedge of unit slope into a wedge of slope $\tan\omega$ through the transformation (see Fig. 1)

$$\left.\begin{aligned} x' &= \frac{k}{k'}x \\ y' &= \frac{k\cos\omega}{k'}(y - z\tan^2\omega) \\ z' &= -\frac{k\sin\omega}{k'}(y+z) \end{aligned}\right\}, \tag{2.8}$$

where

$$k' = \sigma/\sin\omega, \tag{2.9}$$

$$\tan\omega = S(1-\sigma^2)^{-1/2}. \tag{2.10}$$

Eqs. (2.5)–(2.7) become

$$p_{y'y'} + p_{z'z'} - k'^2 p = 0, \tag{2.11}$$

$$p_n = 0 \quad \text{at} \quad z' = -y'\tan\omega, \tag{2.12}$$

$$p_{z'} = p \quad \text{at} \quad z' = 0, \tag{2.13}$$

where the subscript n represents the normal derivative. These equations are identical in form to the equations governing the velocity potential for an inviscid, irrotational surface gravity wave in a homogeneous fluid (e.g., Stoker, 1957), except now the surface and bottom boundaries have been reversed. In Fig. 1, the x', y' and z' axes are drawn for the case $k > 0$. The case $k < 0$ must be excluded for bottom-trapped waves because of the boundary condition (2.13).

In the far field where $y' \gg 1$, the solution to the above equations is approximately given by

$$p = \bar{p}(y')e^{z'},$$

where $\bar{p}$ satisfies

$$\bar{p}_{y'y'} + (1 - k'^2)\bar{p} = 0.$$

These waves can propagate in y' only when

$$k' \leq 1,$$

which can be shown, from (2.9) and (2.10), to be equivalent to

$$\sigma \leq S. \tag{2.14}$$

Since the buoyancy force is the only restoring mechanism in the far field, this criterion is similar to the short-wave cutoff frequency found by Rhines (1970) for bottom-trapped edge waves in an infinitely deep ocean. This cutoff frequency divides the (S,σ) space into two regions as shown in Fig. 2; one region in which waves are progressive in y' and the frequency takes on continuous values, and the other region in which waves are trapped in y' toward the apex of the wedge and the frequency may take on only discrete values.

3. Continuous spectrum

The problem of progressive surface gravity waves impinging on a uniformly sloping beach at an arbitrary incidence angle has been solved by Peters (1952). Since we have shown that the two problems are mathematically identical, his solutions are directly applicable. The two independent standing wave solutions (corresponding to $s = 1$ and 2 in the following expressions) are given by contour integration on the complex ζ plane,

$$\chi_S = (i)^S \times \int_{\Gamma_S} \frac{\zeta g(\zeta,r_1)g(\zeta,r_2)\exp(\eta\zeta + r_1r_2\bar{\eta}/\zeta)d\zeta}{(\zeta + ir_1)(\zeta + ir_2)}, \tag{3.1}$$

where

$$g(\zeta,r) = \exp\left\{-\frac{1}{\pi}\int_0^\infty \frac{\zeta}{v^2 + \zeta^2} \times \ln\left(\frac{v^\mu - r^\mu}{v^\mu}\frac{v^2}{v^2 - r^2}\right)dv\right\} \tag{3.2}$$

is defined in the sector $-\pi/2 - 2\omega < \arg\zeta < \pi/2 + 2\omega$ where it is analytic,

$$\left.\begin{aligned} \eta, \bar{\eta} &= y' \pm iz' \\ r_1, r_2 &= \tfrac{1}{2}[1 \pm (1 - k'^2)^{1/2}] \\ \mu &= \pi/\omega \end{aligned}\right\}, \tag{3.3}$$

and Γ_1, $\Gamma_2 = \Gamma^- \mp \Gamma^+$ are the contours shown in Fig. 3.

Since Peters has shown that these two solutions are sinusoidal in y' and $\pi/2$ radians out of phase

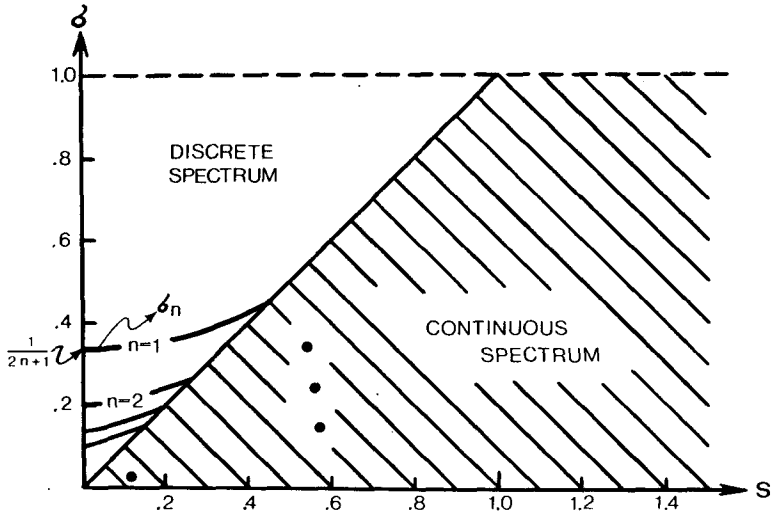

FIG. 2. Separation of (S,σ) space into the regions of continuous and discrete spectrum by the short-wave cutoff. The analytical solution has been numerically evaluated for the cases shown by the solid dots and the eigenfrequencies of the first four trapped modes are shown by the solid curves.

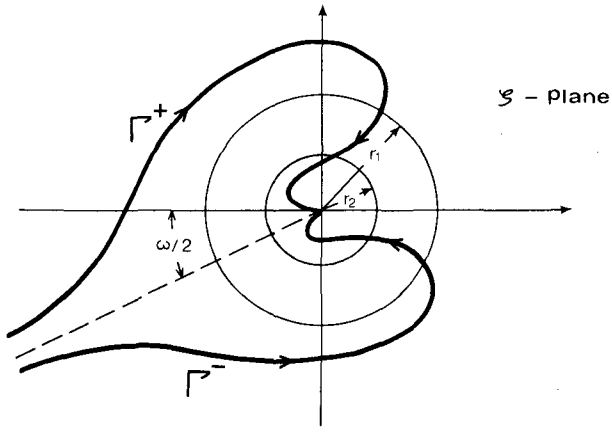

FIG. 3. The contours of integration for the analytical solution of progressive waves.

with each other in the far field, a progressive wave can be constructed from them in a straightforward way.

Before we discuss the general solution (3.1), we will present next the asymptotic solutions for both the far field and small S.

a. Asymptotic solutions

In the far field, the approximate solution of (2.11) through (2.13) is given by

$$p = \exp[z' + i(1 - k'^2)^{1/2}y'], \tag{3.4}$$

or using (2.8),

$$p = \exp\left[-\frac{k\sin\omega}{k'}(y + z) + i\frac{k\cos\omega}{k'}(1 - k'^2)^{1/2}(y - z\tan^2\omega)\right]. \tag{3.5}$$

If not for the hydrostatic balance assumed in our case, this will be the edge wave solution found and discussed to great lengths by Rhines (1970). Without elaborating on the details of the derivation, the following wave properties can be easily observed from (3.5). These waves are bottom trapped with amplitude contours parallel with the bottom, and phase lines tilted from the vertical by an angle that increases for larger S and σ. The bottom trapping is stronger for larger S or smaller σ. Since the frequency depends only on the direction of the wave number vector but not the magnitude of it, the group velocity is perpendicular to the phase velocity. For waves generated from some offshore source, the wave crests must therefore propagate offshore and to the left facing the apex. The angle between the wave crests and the coast is smaller for smaller S and larger σ. The particle motion is rectilinear and straddles the shoreline with the wavenumber vector, giving rise to a negative Reynolds stress. The particle motion becomes more perpendicular to the isobaths when the frequency increases and is more normal than tangential to the isobaths when $\sigma > 0.71S$.

To obtain an asymptotic representation of the solution (3.1) when S is small, we follow closely the method employed by Friedrichs (1948) in the corresponding surface gravity wave problem. Since he has considered the case of normal incidence, an extension of his method is necessary in our case where the incidence angle is arbitrary. Readers are referred to Appendix B for the derivation of the following results.

Let R_Λ and R_A denote the ratio of the cross-wedge wavelength and pressure amplitude to their asymptotic values in the far field. It is shown in Appendix B that

$$R_\Lambda = \lambda(1 - k'^2)^{1/2}/B, \tag{3.6}$$

$$R_A = \tfrac{1}{2}(1 - k'^2)^{1/4}(j(\lambda))^{-1/2} \times \left[\left(\frac{1}{r_1} - \lambda\right)\left(\frac{1}{r_2} - \lambda\right)^{1/2}\left(\frac{1}{r_2} + \lambda\right)^{-1/2} + \left(\frac{1}{r_1} + \lambda\right)\left(\frac{1}{r_2} + \lambda\right)^{1/2}\left(\frac{1}{r_2} - \lambda\right)^{-1/2}\right], \tag{3.7}$$

where r_1, r_2 are given by (3.3),

$$\left.\begin{aligned} j(\lambda) &= AB^{-1}\left(\frac{1}{r_1^2} - \lambda^2\right)\lambda K'(\lambda) \\ K(\lambda) &= BA^{-1}(\tanh^{-1}\lambda r_1 + \tanh^{-1}\lambda r_2) \\ &\quad + \int_0^{\lambda r_1}\tanh^{-1}\nu\,\frac{d\nu}{\nu} \\ &\quad + \int_0^{\lambda r_2}\tanh^{-1}\nu\,\frac{d\nu}{\nu} - \frac{\pi}{2}\ln(r_1 r_2) \\ A &= 1 + r_1 r_2\lambda^2 \\ B &= 1 - r_1 r_2\lambda^2 \end{aligned}\right\}, \tag{3.8}$$

and λ is related to the spatial coordinate y' by

$$Sy' \sim \omega y' = \frac{\lambda}{A}\tanh^{-1}\frac{\lambda}{A}, \tag{3.9}$$

since $\omega \sim S$ in this asymptotic limit.

We plot in Figs. 4 and 5 the contours of constant R_Λ and R_A as functions of k' and $\epsilon = \omega k' y'$. For this asymptotic case we are considering, $k' \approx \sigma/S$, and $\epsilon \approx (Sk)y$ is the distance from the apex multiplied by some constant factor. Fig. 4 shows that the cross-wedge wavelength decreases as the wave approaches the apex. This refraction phenomenon is due primarily to the increased vortex stretching as the water depth decreases. Since the lower frequency waves have their amplitude more confined to the bottom, they don't feel the presence of the upper surface until relatively closer to the apex.

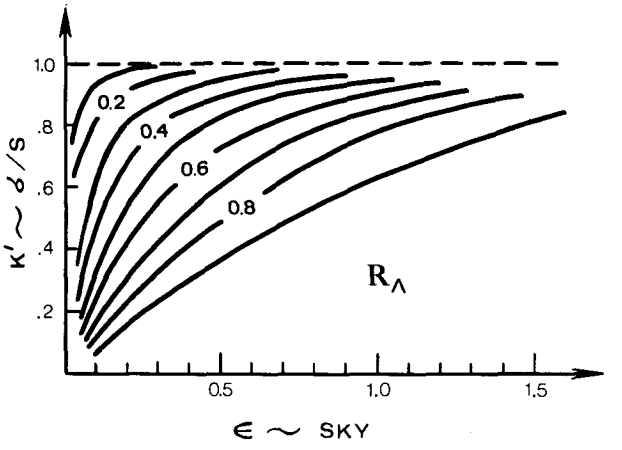

FIG. 4. Contours of R_Λ, the ratio of the cross-wedge wavelength to its asymptotic value in the far-field.

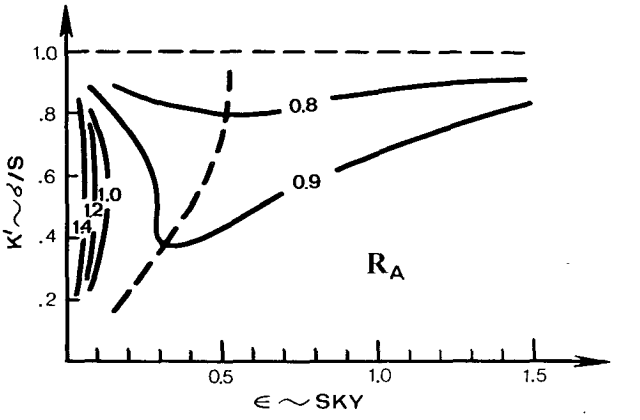

FIG. 5. Contours of R_A, the ratio of pressure amplitude to its asymptotic value in the far field. The thick broken line indicates the location of the minimum.

As a consistency check on the dispersion relation, note that in the far field where $Sy' \gg 1$, (3.9) implies that $\lambda \approx 1/r_1$. From (B.17) in Appendix B, the cross-wedge wavenumber l' is

$$l' = B/\lambda, \tag{3.10}$$

$$\approx (1 - k'^2)^{1/2}, \tag{3.11}$$

which agrees with the solution (3.4).

In the near field, where the motion becomes more barotropic, we expect the local dispersion relation to approach that for barotropic topographic waves. Since $Sy' \ll 1$ in the near field, (3.9) implies that

$$Sy' \approx \lambda^2 \ll 1. \tag{3.12}$$

Using (3.10), (3.12) and (2.8)–(2.10), it is trivial to show that

$$\sigma \approx k/(l^2 y),$$

or in dimensional units

$$\sigma \approx \frac{f \tan\theta^*}{h} \frac{k}{l^2}. \tag{3.14}$$

This is the dispersion relation for barotropic topographic Rossby waves when $l \gg k$ which, of course, holds in the near field. The refraction phenomenon follows clearly from (3.14) which, in addition, shows that $l \sim h^{-1/2}$, i.e., the wavelength decreases as a square root of the local depth.

In Fig. 5, we notice that the wave amplitude goes through a minimum before it becomes infinite near the apex. The singularity at the apex is necessary for the progressive wave solution since all the incoming energy has to be absorbed there without reflection. The presence of amplitude minimum is also commonly observed in the theory of surface gravity waves. Although it is the outcome of the interaction between the incoming bottom intensified waves with the rigid upper surface, the physical basis of it is not clear. Since the lower frequency waves are more isolated from the upper surface, the amplitude minimum is seen to be less pronounced and occurs closer to the apex.

b. The general solution

The general solution (3.1) can be simplified considerably when the transformed slope angle ω equals $\pi/2n$, where n is an integer (see Appendix A for details). The simplified expression is numerically evaluated for the cases shown by the solid dots in Fig. 2. Since the asymptotic solutions for both far field and small S check very well with these calculations, the qualitative behavior of the progressive waves are fairly predictable over the whole range $S \leqslant O(1)$. It is therefore sufficient to present only the solution for the case $n = 3$ and $k' = 0.3$ with k set to 2π, or equivalently $S = 0.57$ and $\sigma = 0.15$.

The normalized pressure field is plotted in Fig. 6, where the solid and broken lines represent the

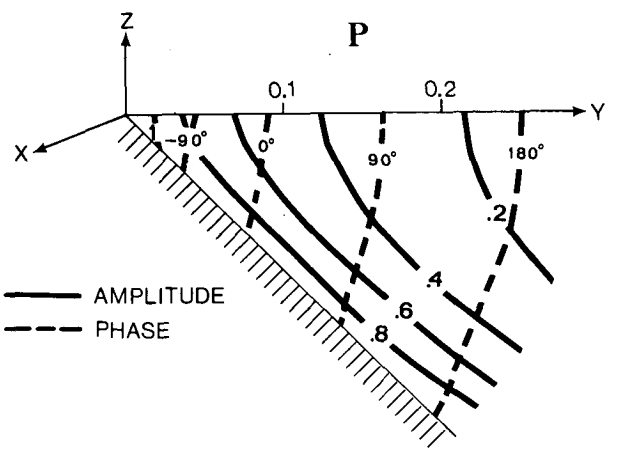

FIG. 6. Analytical solutions of the pressure field for the case $S = 0.57$ and $\sigma = 0.15$, with k set to 2π. Amplitude has been normalized to 1 at the bottom in the far field.

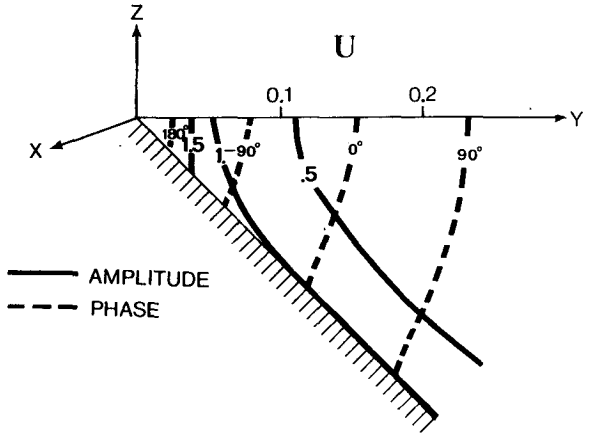

FIG. 7. As in Fig. 6 except for the longshore velocity u.

amplitude and phase contours, respectively. In the far field, consistent with the asymptotic solutions, the waves are bottom intensified with amplitude contours parallel to the bottom, and phase lines tilted from the vertical axis by an angle closely predicted from (3.5). The rigid surface requires that both amplitude and phase contours intersect the surface at right angles. This leads to the more barotropic appearance of the wave amplitude and the more vertical phase lines as the apex is approached. The refraction phenomenon is clearly shown by the shortening of the spacings between phase lines. Along the bottom, the amplitude encounters a minimum before it becomes singular approaching the apex. This minimum has a value of 0.91 and occurs at $y = 0.075$, which agrees with Fig. 5.

The normalized velocities and some other wave properties are plotted in Figs. 7–12. Some simple derivations assuming quasi-geostrophy can help explain the qualitative behavior of these fields. Let

$$p \approx |p|e^{ily},$$

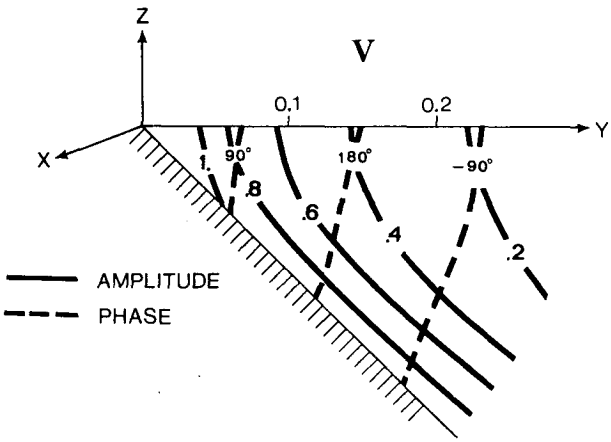

FIG. 8. As in Fig. 6 except for the offshore velocity v. The normalization factor is 0.27 if $|u| = 1$ at the bottom in the far field.

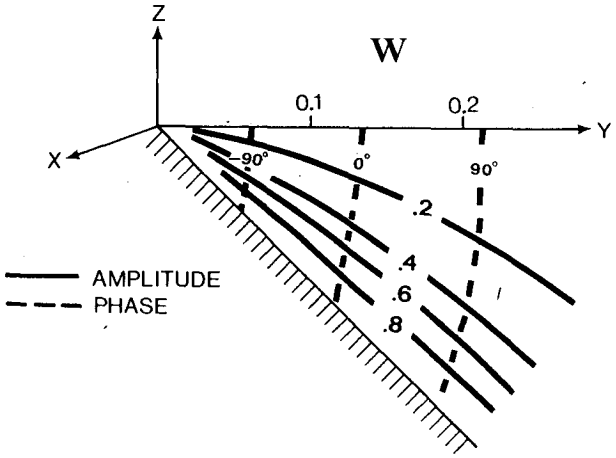

FIG. 9. As in Fig. 6 except for the vertical velocity w. The normalization factor is 0.27.

then quasi-geostrophy implies

$$v = ikp = k|p|e^{i(ly+\pi/2)}, \tag{3.15}$$

$$u = -p_y = (|p|_y^2 + l^2|p|^2)^{1/2} \times \exp\{i[ly + \tan^{-1}(l|p|/|p|_y)]\}. \tag{3.16}$$

As the apex is approached, $|v|$ therefore varies very much like $|p|$, while $|u|$ increases more rapidly due to the combined effect of increasing $|p|_y$ and l. Since $-\pi/2 < \tan^{-1}(l|p|/|p|_y) < 0$, the motion becomes counterclockwisely polarized and the ellipse eccentricity increases moving up the slope. Consistent with the above discussions, the Reynolds stress $\overline{uv}$ is negative and increases in magnitude toward the apex. Because the upper surface is rigid, the phase lines of w are more vertical than those of v. This accounts for the positive $\overline{vp}$ or the onshore heat flux generated by these incoming waves.

4. Discrete spectrum

Stokes (1846) has obtained an edge wave solution for surface gravity waves trapped near the apex of a wedge, and Ursell (1952) has shown that the Stokes' solution is only the fundamental mode ($n = 0$) of a discrete spectrum of possible edge wave modes. With minor modification of Ursell's solution, the solution for the nth mode in our problem is given by

$$p = \exp[-k'(y' \cos\omega - z' \sin\omega)] + \sum_{m=1}^{n} A_{mn} \times \{\exp[-k'(y' \cos(2m-1)\omega + z' \sin(2m-1)\omega)] + \exp[-k'(y' \cos(2m+1)\omega - z' \sin(2m+1)\omega)]\}, \tag{4.1}$$

where

$$A_{mn} = (-1)^m \prod_{l=1}^{m} \frac{\tan(n-l+1)\omega}{\tan(n+l)\omega}, \tag{4.2}$$

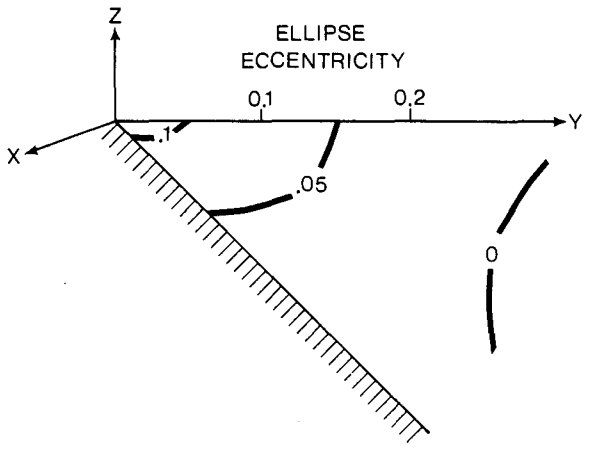

FIG. 10. As in Fig. 6 except for the ellipse eccentricity.

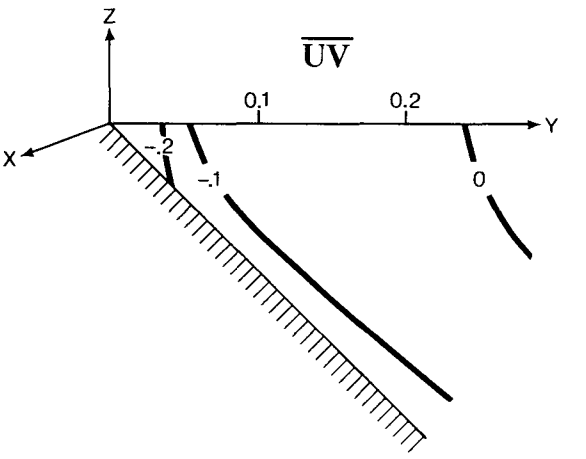

FIG. 11. As in Fig. 6 except for the Reynolds stress $\overline{uv}$. The magnitude has been normalized so that $|u| = 1$ at the bottom in the far field.

and k' and ω satisfy the conditions

$$k' = [\sin(2n + 1)\omega]^{-1}, \tag{4.3}$$

$$\omega \leqslant \omega_c \equiv \pi/[2(2n + 1)]. \tag{4.4}$$

The first condition gives the eigenfrequency of the nth mode,

$$\sigma_n = \sin\omega/\sin(2n + 1)\omega, \tag{4.5}$$

the first four of which are plotted against S in Fig. 2. The second condition is required by the assumption that the solution is coastally trapped and gives the critical value of ω below which the nth mode is allowed. In the limit as S approaches zero, ω is small and

$$\sigma_n \to (2n + 1)^{-1}. \tag{4.6}$$

This agrees with the short-wave limit of Reid's (1958) result for his second class, barotropic edge waves in a wedge. Since Reid retained a free surface in his model, the agreement with our rigid-lid model is expected only for short waves where the surface stretching effect is negligible. The increase of the eigenfrequencies with stratification agrees with the intuition that the stratification imposes an additional restoring force.

In (y,z) space the solution (4.1) becomes

$$p = \exp(-ky) + \sum_{m=1}^{n} A^p_{mn} \exp(-ky\cos2m\omega) \times \cosh(kz\tan\omega\sin2m\omega), \tag{4.7}$$

where

$$A^p_{mn} = 2A_{mn}.$$

The general modal structure of this solution will be discussed next.

Since the consecutive higher terms in the summation decay more slowly in y, they dominate the solution as we move offshore. And since they alternate in sign, nodes are introduced, the number of which equals the mode number n. The modal structure also becomes more bottom trapped offshore because of the increasing depth and the stronger bottom trapping of the higher terms.

The u and v velocities are given by

$$u = \frac{k}{1 + \sigma}[\exp(-ky) + \sum_{m=1}^{n} A^u_{mn} \exp(-ky\cos2m\omega) \times \cosh(kz\tan\omega\sin2m\omega)], \tag{4.8}$$

$$v = \frac{ik}{1 + \sigma}[\exp(-ky) + \sum_{m=1}^{n} A^v_{mn} \exp(-ky\cos2m\omega) \times \cosh(kz\tan\omega\sin2m\omega)], \tag{4.9}$$

where

$$A^u_{mn} = A^p_{mn}(\cos2m\omega - \sigma)/(1 - \sigma), \tag{4.10}$$

$$A^v_{mn} = A^p_{mn}(1 - \sigma\cos2m\omega)/(1 - \sigma). \tag{4.11}$$

Since $A^u_{mn} < A^p_{mn} < A^v_{mn}$, the nodes of u occur farther offshore while those of v occur closer inshore, than the corresponding nodes of p. The first node of

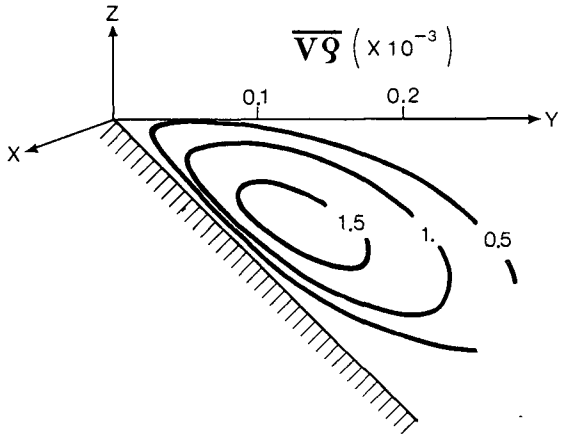

FIG. 12. As in Fig. 11 except for the offshore density flux $\overline{v\rho}$.

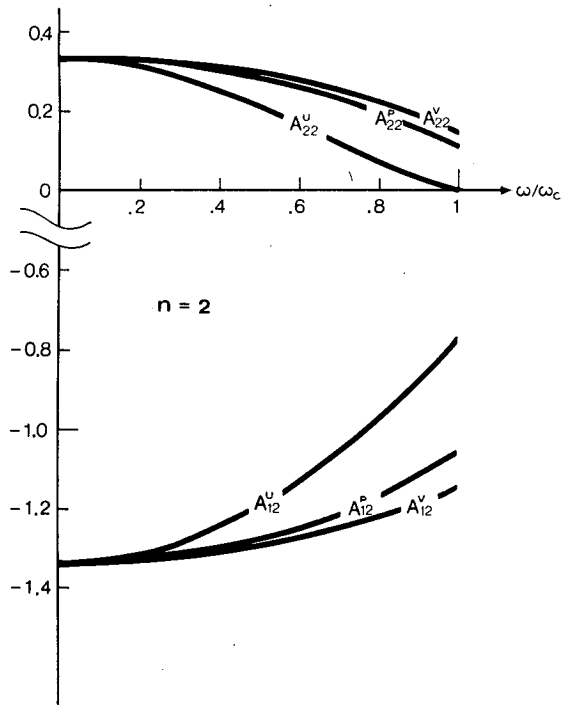

FIG. 13. Values of all the A_{12} and A_{22}'s as a function of ω/ω_c.

v occurs right at the apex due to the impenetrable boundary.

To study the dependence of these modal structures on ω, we plot in Fig. 13, all the A_{mn} values for the second mode. As ω or equivalently S increases, we see that all the A_{mn}'s decrease in magnitude. Since the y-decay rate is also reduced, we infer that the modal structure broadens in y with nodes being pushed offshore. This is clearly shown in Fig. 14 where the nodal positions are plotted. This effect would be the strongest for u which also becomes less depth-dependent than the other variables. In the limit $\omega \to \omega_c$, p and v are no longer coastally trapped, and the second node of u is pushed to infinity since $A^u_{22} \to 0$.

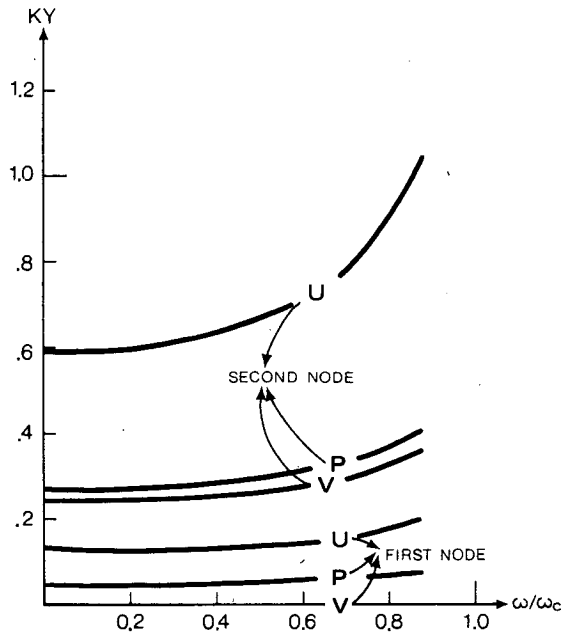

FIG. 14. Nodal positions of p, u and v for the second trapped mode, as a function of ω/ω_c.

Acknowledgments. The author is very grateful to Dr. Robert Beardsley for carefully reading the manuscript and his many suggestions that greatly improved the clarity of this paper. Thanks are also extended to Dr. Peter Rhines and Dr. Nelson Hogg for many helpful discussions.

This work has been supported at the Woods Hole Oceanographic Institution by the National Science Foundation under Grants OCE 76-01813 and OCE 78-19513.

APPENDIX A

Reduction of the Analytical Solution

The analytical solution (3.1) can be simplified when $\omega = \pi/2n$ where n is an integer. Peters (1952) showed that with $h(\zeta)$ defined by

$$h(\zeta) = \zeta g(\zeta,r)/(\zeta + ir), \tag{A1}$$

where $g(\zeta,r)$ is given by (3.2), then $I(\zeta) \equiv \ln h(\zeta)$ satisfies

$$I(\zeta e^{i\omega},r) = -\frac{1}{\pi}\int_0^\infty \frac{\zeta}{v^2+\zeta^2}\ln\left[1+\left(\frac{r}{v}\right)^{2n}\right]dv$$

for

$$-\frac{\pi}{2} < \arg\zeta < \frac{\pi}{2}. \tag{A2}$$

When $\omega = \pi/2n$, Eq. (A2) becomes

$$I(\zeta e^{i\pi/2n},r) = -\frac{1}{2\pi}\int_{-\infty}^\infty \frac{\zeta}{v^2+\zeta^2}\ln\left[1+\left(\frac{r}{v}\right)^{2n}\right]dv$$

$$= -\frac{1}{2\pi i}\int_{-\infty}^\infty \frac{1}{v-i\zeta}\ln\left[1+\left(\frac{r}{v}\right)^{2n}\right]dv$$

$$= -\frac{n}{\pi i}\int_{-\infty}^\infty \frac{\ln(v-i\zeta)dv}{v\left[1+\left(\frac{r}{v}\right)^{2n}\right]} \quad \text{(integration by parts)}$$

$$= -\frac{n}{\pi i}\int_{-\infty}^\infty \frac{\ln(ru-i\zeta)du}{u[1+u^{2n}]} \quad (u \equiv v/r)$$

$$= n\ln(-i\zeta) + 2n \times \sum_{k=1}^{n} \frac{\ln(ru_k - i\zeta)}{u_k \prod_{\substack{k'=1 \\ k'\neq k}}^{2n}(u_k - u_{k'})} \quad \text{(residue theorem)} \tag{A3}$$

where

$$u_k = \exp[-i\pi(2k-1)/2n], \quad k = 1, \ldots, 2n.$$

Since it can be trivially shown that

$$u_k \prod_{\substack{k'=1 \\ k' \neq k}}^{2n} (u_k - u_{k'}) = -2n,$$

Eq. (A3) implies

$$I(\zeta e^{i\pi/2n}, r) = n \ln(-i\zeta) - \sum_{k=1}^{n} \ln(ru_k - i\zeta), \quad \text{(A4)}$$

or

$$I(\zeta,r) = \ln \frac{\zeta^n \exp[-i\pi(1+n)/2]}{\prod_{k=1}^{n} \{ru_k + \zeta \exp[-i\pi(1+1/n)/2]\}}, \quad \text{(A5)}$$

or

$$\frac{g(\zeta,r)}{\zeta + ir} = \frac{\zeta^{n-1} \exp[-i\pi(1+n)/2]}{\prod_{k=1}^{n} \{ru_k + \zeta \exp[-i\pi(1+1/n)/2]\}} = \frac{\zeta^{n-1}}{\prod_{k=1}^{n} (\zeta - r\zeta_k)}, \quad \text{(A6)}$$

where

$$\zeta_k = \exp\left[i\pi\left(\frac{1}{2} + \frac{k}{n}\right)\right].$$

Substituting (A6) into (3.1) yields

$$\chi_S = (i)^S \int_{\Gamma_S} \frac{\zeta^{2n-1} \exp(\eta\zeta + r_1 r_2 \bar{\eta}/\zeta) d\zeta}{\prod_{k=1}^{n} (\zeta - r_1\zeta_k)(\zeta - r_2\zeta_k)}. \quad \text{(A7)}$$

The evaluation of χ_1 can be reduced to a summation of its residues using the residue theorem, but the evaluation of χ_2 involves contour integration which must be numerically calculated.

APPENDIX B

Asymptotic Solution for Small S

Since the derivation below follows very closely that of Friedrichs (1948), we will only write down some key results and the corresponding equation number in Friedrichs' paper (preceded by a capital F).

Let

$$\chi_\pm \equiv \int_{\Gamma_\pm} \frac{\zeta^{2n-1} \exp(\eta\zeta + r_1 r_2 \bar{\eta}/\zeta) d\zeta}{\prod_{k=1}^{n} (\zeta - r_1\zeta_k)(\zeta - r_2\zeta_k)}, \quad \text{(B1),(F3)}$$

where all the notations have been defined in (3.3) and Appendix A. Then $\chi_{1,2}$ of (A7) are simply given by

$$\left.\begin{aligned} \chi_1 &= i(\chi_+ - \chi_-) \\ \chi_2 &= \chi_+ + \chi_- \end{aligned}\right\}. \quad \text{(B2),(F8)}$$

In the limit $n \to \infty$, (B1) becomes

$$\chi_\pm \sim -\int_{\Gamma_\pm} \frac{1}{\zeta} (r_1 r_2)^{-n} \left(\frac{1}{\zeta} + \frac{i}{r_1}\right)^{1/2} \left(\frac{1}{\zeta} + \frac{i}{r_2}\right)^{1/2} \times \left(\frac{1}{\zeta} - \frac{i}{r_1}\right)^{-1/2} \left(\frac{1}{\zeta} - \frac{i}{r_2}\right)^{-1/2} \times \exp\left[\eta\zeta + r_1 r_2 \bar{\eta}/\zeta - \frac{1}{\omega}(H(\zeta,r_1) + H(\zeta,r_2))\right] d\zeta, \quad \text{(B3),(F22)}$$

where

$$H(\zeta,r) = \int_0^{1/\zeta} \tan^{-1}(\mu r) \cdot \frac{d\mu}{\mu} - \frac{\pi}{2} \ln r. \quad \text{(B4),(F26)}$$

The saddle point $\tilde{\zeta}$ is given by

$$\omega y' = [H'(\tilde{\zeta},r_1) + H'(\tilde{\zeta},r_2)]/(1 - r_1 r_2/\zeta^2), \quad \text{(B5),(F44)}$$

or by setting $\tilde{\zeta} \equiv i\lambda^{-1}$,

$$\omega y' = \lambda A^{-1}(\tanh^{-1}\lambda r_1 + \tanh^{-1}\lambda r_2), \quad \text{(B6),(F46)}$$

where

$$A = 1 + r_1 r_2 \lambda^2, \quad \text{(B7)}$$

$$B = 1 - r_1 r_2 \lambda^2. \quad \text{(B8)}$$

The solution (B3) can then be approximated by,

$$\chi_\pm \sim (r_1 r_2)^{-n} \left(\frac{1}{r_1} \mp \lambda\right)\left(\frac{1}{r_2} \mp \lambda\right)^{1/2} \times \left(\frac{1}{r_2} \pm \lambda\right)^{-1/2} (2m\omega)^{1/2} (j(\lambda))^{-1/2} \times \exp\left[\pm i\omega^{-1} K(\lambda) \pm i\frac{\pi}{4}\right], \quad \text{(B9),(F52)}$$

where

$$j(\lambda) = AB^{-1}\left(\frac{1}{r_1^2} - \lambda^2\right)\lambda K'(\lambda), \quad \text{(B10),(F49)}$$

$$K(\lambda) = BA^{-1}(\tanh^{-1}\lambda r_1 + \tanh^{-1}\lambda r_2) + \int_0^{\lambda r_1} \tanh^{-1}\nu \frac{d\nu}{\nu} + \int_0^{\lambda r_2} \tanh^{-1}\nu \frac{d\nu}{\nu} - \frac{\pi}{2} \ln(r_1 r_2). \quad \text{(B11),(F48)}$$

In the far field, where $\omega y' \gg 1$, Eq. (B9) becomes

$$\chi_+ \sim 2(r_1 r_2)^{-n} \exp(-2C\omega y')(1 - k'^2)^{1/4} (2\pi\omega)^{1/2} \times \exp i\left[(1 - k'^2)^{1/2} y' + \frac{D}{\omega} + \frac{\pi}{4}\right], \quad \text{(B12),(F67)}$$

$$\chi_- \sim 2(r_1 r_2)^{-n}(1 - k'^2)^{1/4}(2\pi\omega)^{1/2}$$

$$\times \exp\left\{-i\left[(1 - k'^2)^{1/2}y' + \frac{D}{\omega} + \frac{\pi}{4}\right]\right\}, \quad \text{(B13),(F68)}$$

where

$$C = r_1 + r_2,$$

$$D = \left(\frac{r_1 - r_2}{r_1 + r_2} + \frac{r_2^2 - r_1^2}{2r_1^2}\right)\tanh^{-1}\frac{r_2}{r_1} + \frac{r_2}{2r_1} - \frac{\pi}{2}\ln(r_1 r_2).$$

Accordingly, Eq. (B2) implies

$$\chi_{1,2} \sim \mp 2(r_1 r_2)^{-n}(1 - k'^2)^{1/4}(2\pi\omega)^{1/2}$$

$$\times \exp\left\{-i\left[(1 - k'^2)^{1/2}y' + \frac{D}{\omega} \mp \frac{\pi}{4}\right]\right\}. \quad \text{(B14),(F69)}$$

The two solutions are sinusoidal and differ in phase by 90°.

We define the "local" cross-wedge wavelength as

$$\Lambda' = 2\pi\left[\frac{d}{dy'}\,\omega^{-1}K(\lambda)\right]^{-1} \quad \text{(B15),(F31)}$$

$$= 2\pi\lambda/B, \quad \text{(B16),(F32)}$$

then the local cross-wedge wavenumber is given by

$$l' = 2\pi/\Lambda' = B/\lambda. \quad \text{(B17)}$$

The local amplitude can also be derived

$$A_m(\lambda) = \left[(r_1^{-1} - \lambda)\left(\frac{r_2^{-1} - \lambda}{r_2^{-1} + \lambda}\right)^{1/2} + (r_1^{-1} + \lambda)\left(\frac{r_2^{-1} + \lambda}{r_2^{-1} - \lambda}\right)^{1/2}\right]\left(\frac{2m\omega}{j(\lambda)}\right)^{1/2}. \quad \text{(B18),(F13)}$$

From (B14), we can then derive that

$$R_\Lambda = \Lambda/\Lambda]_\infty = \lambda(1 - k'^2)^{1/2}/(1 - \tfrac{1}{4}k'^2\lambda^2), \quad \text{(B19)}$$

$$R_A = A_m/A_m]_\infty = \tfrac{1}{2}(1 - k'^2)^{1/4}(j(\lambda))^{1/2}(r_1^{-1} - \lambda)\left(\frac{r_2^{-1} - \lambda}{r_2^{-1} + \lambda}\right)^{1/2} + (r_1^{-1} + \lambda)\left(\frac{r_2^{-1} + \lambda}{r_2^{-1} - \lambda}\right)^{1/2}. \quad \text{(B20)}$$

REFERENCES

Friedrichs, K. O., 1948: Water waves on a shallow sloping beach. *Commun. Pure Appl. Math.*, **1**, 109–134.

Huthnance, J. M., 1978: On coastal trapped waves: Analysis and numerical calculation by inverse iteration. *J. Phys. Oceanogr.*, **8**, 74–92.

Ou, H. W., and R. C. Beardsley, 1980: On the propagation of free topographic Rossby waves near continental margins. Part 2: Numerical model. *J. Phys. Oceanogr.*, **10** (in press).

Peters, A. S., 1952: Water waves over sloping beaches and the solution of a mixed boundary value problem for $\Delta\varphi - k^2\varphi = 0$ in a sector. *Commun. Pure Appl. Math.*, **5**, 87–108.

Reid, R. O., 1958: Effect of Coriolis force on edge waves, (1) investigation of the normal modes. *J. Mar. Res.*, **16**, 109–144.

Rhines, P. B., 1970: Edge-, bottom-, and Rossby waves in a rotating stratified fluid. *Geophys. Fluid Dyn.*, **1**, 273–302.

——, 1971: A note on long period motions at site D. *Deep-Sea Res.*, **18**, 21–26.

Stoker, J. J., 1957: *Water Waves*. Interscience, 567 pp.

Stokes, G. G., 1846: Report on recent researches in hydrodynamics. *Brit. Assoc. Rep.*, 1–20.

Thompson, R. O. R. Y., 1971: Topographic Rossby waves at a site north of the Gulf Stream. *Deep-Sea Res.*, **23**, 629–635.

——, 1977: Observations of Rossby waves near Site D. *Progress in Oceanography*, Vol. 7, Pergamon Press, 1–28.

——, and J. R. Luyten, 1976: Evidence for bottom-trapped topographic Rossby waves from single moorings. *Deep-Sea Res.*, **23**, 629–635.

Ursell, F., 1952: Edge waves on a sloping beach. *Proc. Roy. Soc. London*, **A214**, 79–97.

Wang, D. P., and C. N. K. Mooers, 1976: Coastal-trapped waves in a continuously stratified ocean. *J. Phys. Oceanogr.*, **6**, 853–863.